4-27-2000

A Free Moving Boundary Model and Boundary Iteration Method for Unsteady Viscous Flow in Stenotic Elastic Tubes

Dalin Tang
Worcester Polytechnic Institute, dtang@wpi.edu

Jun Yang

Suggested Citation

Tang, D., & Yang, J. (2000). A Free Moving Boundary Model and Boundary Iteration Method for Unsteady Viscous Flow in Stenotic Elastic Tubes. *SIAM Journal on Scientific Computing*, *21*(4), 1370-1386. http://dx.doi.org/10.1137/S1064827597315686

SIAM J. SCI. COMPUT.
Vol. 21, No. 4, pp. 1370–1386

A FREE MOVING BOUNDARY MODEL AND BOUNDARY ITERATION METHOD FOR UNSTEADY VISCOUS FLOW IN STENOTIC ELASTIC TUBES*

DALIN TANG† AND JUN YANG†

Abstract. A nonlinear mathematical model with a free moving boundary was introduced to study viscous flow in stenotic elastic tubes subject to a prescribed external pressure at the tube wall and pulsatile pressure drop between the tube inlet and outlet. An iterative numerical method using boundary iteration, pseudocompressibility, and the ADI technique was developed to solve the model. Unsteady effects of stenosis severity and the imposed pressure conditions on the tube wall and flow are studied. Special attention was paid to tube contractions because they can be indications of the tube collapsing. It was found that stenosis can cause more severe tube expansion and contraction under unsteady conditions. The complicated unsteady wall motion can be understood as the superposition of the static tube expansion and contraction caused by the stenosis and as the unsteady tube expansion and contraction caused by the imposed, unsteady pressure conditions.

Key words. collapsible, stenotic, free boundary, moving boundary, Navier–Stokes, viscous

AMS subject classifications. 76, 39, 41, 34

PII. S1064827597315686

1. Introduction and literature review.

Nonlinear viscous flow with free moving boundaries (FmBs) has attracted the interest of many researchers in the field of computational fluid dynamics in recent years and has many interesting and important engineering applications. Various numerical methods have been developed to deal with the nonlinearity of the problem and the coupling of the pressure with flow velocities. Detailed reviews of these methods can be found in [17, 10]. The perturbation method, potential theory, and computational tools have been applied to two-dimensional inviscid flows with free surfaces [20, 21]. Peskin [12, 13] introduced the immersed boundary method and his fiber concept to investigate blood flow in the heart, which was treated as an FmB, and his success is well recognized around the world. Fauci [4] applied the immersed boundary method to peristaltic pumping of solid particles and studied the motion of the particles. Roser [14] developed a full three-dimensional model and solved it using the immersed boundary method to investigate flow in collapsible tubes without stenoses, obtaining interesting results. By using two layers of fibers to construct the tube wall, Rosar's model has the potential to handle the complicated mechanical properties of blood vessels.

In this paper, a boundary iteration method is introduced to study nonlinear viscous flow in elastic collapsible tubes with stenosis (see Figure 1). The method is explained in detail in section 3. The problem considered in this paper has important applications in biomedical engineering, especially for blood flow in arteries with stenosis [7, 8, 9, 2, 3]. An "artery collapsing theory" is as follows. Blood flow must accelerate to high velocities in the narrowed stenosis. The high velocities in turn create a low or negative transmural pressure that can result in collapse of the artery. The resultant flow restriction during collapse may lead directly to heart attack and stroke. A

*Received by the editors January 27, 1997; accepted for publication (in revised form) October 9, 1998; published electronically February 2, 2000. This research was supported in part by National Science Foundation grant DMS–9505685 and by a grant from the Whitaker Foundation.
http://www.siam.org/journals/sisc/21-4/31568.html
†Department of Mathematical Sciences, Worcester Polytechnic Institute, Worcester, MA 01609 (dtang@math.wpi.edu, junyang@math.wpi.edu).

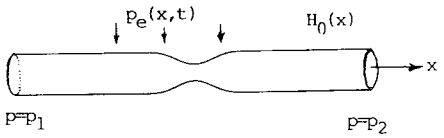

FIG. 1. *Resting shape of the stenotic elastic tube.*

better understanding of this complicated physiological process is of great importance to the early diagnosis, prevention, and treatment of stenosis-related diseases.

Current mathematical models for flow in collapsible tubes with stenosis are primarily limited to one-dimensional models [9, 3, 15, 6] because of the difficulty of handling the collapsible tubes which must be treated as FMBs. The accuracy of such models is limited because only the average axial velocity and pressure over the cross section of the tube are calculated. Higher dimensional models need to be developed to investigate the collapsing phenomena and to provide computational results, which are hard to get from either experimental data or one-dimensional models.

We introduce a nonlinear mathematical model to study unsteady viscous flow in axisymmetric elastic tubes with stenoses subjected to a time-dependent external pressure imposed on the tube wall and pulsatile pressure drop imposed between the inlet and outlet of the tube. The tube law introduced by Shapiro [15] was adapted to reflect the interaction between the tube wall and the flow. Effects of the severity of stenoses and the imposed pressure conditions on the tube wall motion and flow were investigated by studying the free moving boundaries, flow velocities, shear stress fields, flux, etc. Special attention was given to tube contraction because it is an indication of possible tube collapsing. The axisymmetric model and its solutions should provide a basis for a better understanding of the prebuckling stage of nonlinear viscous flow in stenotic collapsible tubes. It is also a necessary preparation for the full three-dimensional investigation of the collapsing process.

2. Formulation of the mathematical model. We consider unsteady viscous flow in an axisymmetric stenotic elastic tube whose shape is to be determined (Figure 1). The flow is assumed to be laminar, axisymmetric, Newtonian, viscous, and incompressible. The Navier–Stokes equations were used as the governing equations. The tube wall is assumed to be axisymmetric with an attached stenosis. For boundary conditions, we assume that the tube wall has no axial motions, that no slipping takes place between the fluid and the wall, and that no penetration of the fluid through the tube wall occurs. The tube law [15] is adapted in this paper to reflect the interaction between the wall and the fluid. An external pressure is prescribed at the wall and a pulsatile pressure drop is imposed between the inlet and outlet of the tube. These lead to the following model:

$$u_t + uu_x + vu_r = -\frac{1}{\rho}p_x + \nu\nabla^2 u, \tag{2.1}$$

$$v_t + uv_x + vv_r = -\frac{1}{\rho}p_r + \nu\left(\nabla^2 v - \frac{v}{r^2}\right) \qquad \text{(Navier–Stokes equations)}, \tag{2.2}$$

$$u_x + \frac{v}{r} + v_r = 0, \tag{2.3}$$

$$\Gamma : r = H(x,t) = H_0(x) + H_c(x,t) \qquad \text{(tube wall, the FMBs)}, \tag{2.4}$$

$$(u,v)|_\Gamma = \left(0, \frac{\partial H}{\partial t}\right) \qquad \text{(boundary condition)}, \tag{2.5}$$

$$p - p_e|_\Gamma = K_p\left[\left(\frac{H}{H_0}\right)^{2n_1} - \left(\frac{H}{H_0}\right)^{-2n_2}\right] \qquad \text{(tube law)}, \tag{2.6}$$

$$p|_{x=0} = p_e(0,t), \qquad p|_{x=\ell} = p_e(\ell,t) \qquad \text{(inlet-outlet pressure)}, \tag{2.7}$$

$$H|_{t=0} = H_i, \qquad (u,v)|_{t=0} = (u_i, v_i), \qquad p|_{t=0} = p_i \qquad \text{(initial condition)}, \tag{2.8}$$

where

$$\nabla^2 = \frac{\partial^2}{\partial x^2} + \frac{\partial^2}{\partial r^2} + \frac{1}{r}\frac{\partial}{\partial r},$$

$\mathbf{u} = (u,v)$, u and v are the axial and radial components of the flow velocity, respectively, p is the pressure, ρ is fluid density, and ν is the kinematic viscosity. Γ stands for the tube wall, where $H(x,t)$ is the radius of the tube to be determined as part of the solution, ℓ is the tube length, $H_0(x)$ gives the shape of the tube under zero transmural pressure,

$$H_0(x) = R_0 - S(x) \qquad \text{(tube at rest)}, \tag{2.9}$$

$S(x)$ specifies the shape of the stenosis, R_0 is the radius of the nonstenotic part of the tube at rest, $p_e(x,t)$ is the prescribed external pressure, $H_c(x,t)$ is the variation of the tube radius caused by nonzero transmural pressure,

$$p_{\text{tran}} = p|_\Gamma - p_e \qquad \text{(transmural pressure)}, \tag{2.10}$$

K_p is the stiffness of the tube wall, which can vary with x because of the presence of the stenosis, n_1 and n_2 are two stiffness parameters for the tube, and T is the time period of the imposed pressure conditions. The pressure drop p_d is defined as

$$p_d = p|_{x=0} - p|_{x=\ell} \qquad \text{(pressure drop)}. \tag{2.11}$$

Introducing the following new variables and parameters,

$$\begin{aligned}
&t^* = \frac{t}{T}, \qquad (x^*, r^*) = \frac{(x,r)}{D}, \qquad \ell^* = \frac{\ell}{D},\\
&H^* = \frac{H}{D}, \qquad S^* = \frac{S}{D}, \qquad H_c^* = \frac{H_c}{D}, \qquad H_0^* = \frac{H_0}{D}, \qquad R_0^* = \frac{R_0}{D},\\
&(u^*, v^*) = \frac{(u,v)}{U}, \qquad p^* = \frac{p}{(\rho U^2)}, \qquad p_e^* = \frac{p_e}{(\rho U^2)}, \qquad p_d^* = \frac{p_d}{(\rho U^2)},\\
&K_p^* = \frac{K_p}{(\rho U^2)}, \qquad R = \frac{UD}{\nu}, \qquad \alpha_w = D\left(\frac{\omega}{\nu}\right)^{\frac{1}{2}} = D\left(\frac{2\pi}{T\nu}\right)^{\frac{1}{2}}
\end{aligned} \tag{2.12}$$

and dropping all the *s, we obtain the nondimensionalized model:

$$\frac{\alpha_w^2}{2\pi R}u_t + uu_x + vu_r = -p_x + \frac{1}{R}\nabla^2 u, \tag{2.13}$$

$$\frac{\alpha_w^2}{2\pi R}v_t + uv_x + vv_r = -\frac{1}{\rho}p_r + \frac{1}{R}\left(\nabla^2 v - \frac{v}{r^2}\right) \quad \text{(Navier–Stokes equations)}, \tag{2.14}$$

$$u_x + \frac{v}{r} + v_r = 0, \tag{2.15}$$

$$\Gamma : r = H(x,t) + H_0(x) + H_c(x,t), \quad 0 \le x \le \ell \qquad \text{(tube wall)}, \tag{2.16}$$

$$(u,v)|_\Gamma = \left(0, \frac{\alpha^2}{2\pi R}\frac{\partial H}{\partial t}\right) \qquad \text{(boundary condition)}, \tag{2.17}$$

$$p - p_e|_\Gamma = K_p\left[\left(\frac{H}{H_0}\right)^{2n_1} - \left(\frac{H}{H_0}\right)^{-2n_2}\right] \qquad \text{(tube law)}, \tag{2.18}$$

$$p|_{x=0} = p_e(0,t), \qquad p|_{x=\ell} = p_e(\ell,t) \qquad \text{(inlet-outlet pressure)}, \tag{2.19}$$

$$H|_{t=0} = H_i, \qquad (u,v)|_{t=0} = (u_i, v_i), \qquad p|_{t=0} = p_i \qquad \text{(initial conditions)}, \tag{2.20}$$

where U, D, and T are units for velocity, spatial coordinates, and time, respectively, R is the Reynolds number, and α_w is the Womersely number. In this paper, we set

$$S(x) = \begin{cases} S_0 R_0[1 - \cos(2\pi(x - x_1)/(x_2 - x_1))]^{\frac{2}{4}}, & x_1 \le x \le x_2 \\ 0 \qquad \text{otherwise}, \end{cases} \qquad \text{(stenosis)}, \tag{2.21}$$

where S_0 gives the severity of the stenosis, and x_1 and x_2 specify the position and length of it.

Corresponding to the stenosis described by $S(x)$, we have

$$K_p = K_{pi}\big(1 + \lambda_{kp}S(x)\big), \tag{2.22}$$

where λ_{kp} is the amplitude of the stiffness perturbation, which is set to be 0.5, 0.0, and -0.5, corresponding to three kinds of stenoses introduced in [9]. K_{pi} is proportional to [9]

$$\frac{Eh^3}{12R_0^3(1-\nu^2)}, \tag{2.23}$$

where E is Young's modulus, h is the tube wall thickness, and ν is Poisson's ratio. (Elsewhere in this paper, ν always stands for the kinematic viscosity.)

The external pressure and pressure-drop conditions are prescribed as

$$p_e = p_0 - \frac{x}{\ell}p_{do} + \frac{\ell - x}{\ell}p_{do}A_{pe}\sin\frac{2\pi x}{\ell - 2\pi t} \qquad \text{(external pressure)}, \tag{2.24}$$

$$p|_{x=0} = p_e(0,t) = p_0 - p_{do}A_{pe}\sin(2\pi t) \qquad \text{(inlet pressure)}, \tag{2.25}$$

$$p|_{x=\ell} = p_e(\ell,t) = p_0 - p_{do} \qquad \text{(outlet pressure)}, \tag{2.26}$$

$$p_d(t) = p_{do}[1 - A_{pe}\sin(2\pi t)] \qquad \text{(pressure drop)}, \tag{2.27}$$

where p_0 is the mean inlet pressure, p_{do} is the mean pressure drop in time, and A_{pe} is the relative amplitude of the unsteady pressure drop. By setting the internal pressure equal to the imposed external pressure at the inlet and outlet, we are setting the inlet and outlet of the tube equally and not moving with time. The periodicity of the imposed pressure conditions in x implies the periodicity of the tube and flow velocity, i.e.,

$$H|_{x=0} = H|_{x=\ell} = R_0 \qquad \text{(periodicity of } H\text{)}, \tag{2.28}$$

$$\mathbf{u}|_{x=0} = \mathbf{u}|_{x=\ell} \qquad \text{(periodicity of } u\text{)}. \tag{2.29}$$

The mathematical model is complete.

3. Longwave approximation. Assuming $1/\ell \ll 1$ and following the standard procedure [18], we obtained the longwave approximations (still use u, v, p, H for the zeroth-order approximations u_0, v_0, H^0, p^0)

$$u = 0.25R\big(r^2 - H^2\big)p_x, \tag{3.1}$$

$$v = .025rR\big[HH_x p_x - p_{xx}\big(0.25r^2 - 0.5H^2\big)\big] \qquad \text{(longwave approximation)}, \tag{3.2}$$

$$p = p_e + K_p\left[\left(\frac{H}{H_0}\right)^{2n_1} - \left(\frac{H}{H_0}\right)^{-2n_2}\right], \tag{3.3}$$

where the free boundary $H(x)$ can be determined from

$$\frac{dH}{dx} = \frac{\overline{C}H_0^2 + K_p M(\alpha)H^5\big(\frac{dH_0}{dx}\big) - \big(\frac{dp_e}{dx}\big)H^4H_0^2 - \big(\frac{dK_p}{dx}\big)H^4H_0^2N(\alpha)}{K_p M(\alpha)H^4H_0}, \tag{3.4}$$

$$H(0) = H(1) = R_0, \tag{3.5}$$

where

$$\overline{C} = R_0^4 p_x(0), \qquad \alpha = \frac{H}{H_0}, \tag{3.6}$$

$$M(\alpha) = 2n_1\alpha^{2n_1-1} + 2n_2\alpha^{-2n_2-1}, \qquad N(\alpha) = n_1\alpha^{2n_1} - n_2\alpha^{-2n_2}, \tag{3.7}$$

and $p_x(0)$ is a constant to be determined with the solution. It can be shown similar to [18] that (3.4)–(3.5) has a unique solution under some conditions on these parameters.

4. The numerical method. The nonlinear mathematical model was solved by using a boundary iteration method [18, 19] that can be explained in the steps as follows:

Step 1. Obtain the longwave solution of the steady model and use it as the initial condition of the unsteady numerical model.

Step 2. Discretize the model. For each time step $t = t_i$, do the following:

(a) Use the solutions at the previous time step as the numerical initial condition for the current time step.

(b) Use the tube law and the current p and $p_e(x, t_i)$ to determine $H(x, t_i)$.

(c) Use the boundary $r = H(x, t_i)$ and the mapping

$$\xi = x, \quad \eta = \frac{r}{H(x, t_i)}, \qquad t = t \tag{4.1}$$

to map the (x, r, t)-domain into a rectangular (ξ, η, t)-domain.

(d) Use the alternating direction implicit (ADI) method to solve u and v and a pseudocompressibility method to obtain p.

(e) Check the relative residuals of all the equations and the tube law.

(f) Repeat (b)–(e) until desired accuracy is reached, then move to the next time step.

Step 3. Repeat Step 2 until the final time step is reached.

Remark. The intuitive idea for the boundary iteration method was mentioned by Fung [5, p. 91]. This method is a technique to deal with problems with free moving boundaries. By using the boundary iterations, the unknown boundary becomes "known" at each iteration step so that the Navier–Stokes equations can be solved over

a "known" domain. The ADI method was used to reduce the inversion of a formidable matrix inversion problem resulting from the discretization of the Navier–Stokes equations to the inversion of two tridiagonal matrices. The pseudocompressibility method is a popular technique developed to couple the pressure with velocity by introducing an artificial compressibility into the system. The incompressibility is recovered as the algorithm converges. More details about the ADI and pseudocompressibility methods can be found in the monograph by Kwak [10].

The iterative numerical scheme. The time derivatives in the momentum equations can be differenced using a second-order three-point implicit formula [10],

$$\frac{d\mathbf{u}}{dt} = \frac{1.5\mathbf{u}^{n+1} - 2u^n + 0.5\mathbf{u}^{n-1}}{\Delta t}. \tag{4.2}$$

A pseudotime derivative of the pressure is added to couple the pressure and the velocity,

$$\frac{\partial p}{\partial \sigma} = -\beta\left(u_x + \frac{v}{r} + v_r\right), \tag{4.3}$$

where β is the artificial compressibility. When the algorithm is converging, (4.3) implies

$$u_x + \frac{v}{r} + v_r \to 0. \tag{4.4}$$

With a two-point differencing for $\partial/\partial\sigma$ and using m for pseudotime step, under the mapping (4.1), the Navier–Stokes equations in terms of (ξ, η) can be written as

$$\begin{aligned}
&\frac{\alpha_w^2}{2\pi R}\frac{1.5u^{n+1,m+1} - 2u^n + 0.5u^{n-1}}{\Delta t} \\
&\quad = \frac{1}{R}\Big[u_{\xi\xi}^{n+1,m+1} + 2u_{\xi\eta}^{n+1,m+1}\eta_x + u_{\eta\eta}^{n+1,m+1}\big(\eta_x^2 + \eta_r^2\big) \\
&\qquad + u_\eta^{n+1,m+1}\eta_{xx} + \frac{1}{r}u_\eta^{n+1,m+1}\eta_r\Big] \\
&\qquad - u^{n+1,m}\big(u_\xi^{n+1,m+1} + u_\eta^{n+1,m+1}\eta_x\big) - v^{n+1,m}u_\eta^{n+1,m+1}\eta_r \\
&\qquad - \big(p_\xi^{n+1,m} + p_\eta^{n+1,m}\eta_x\big) - \frac{\alpha_w^2}{2\pi R}u_\eta^{n+1,m}\eta_t,
\end{aligned} \tag{4.5}$$

$$\begin{aligned}
&\frac{\alpha_w^2}{2\pi R}\frac{1.5v^{n+1,m+1} - 2v^n + 0.5v^{n-1}}{\Delta t} \\
&\quad = \frac{1}{R}\Big[v_{\xi\xi}^{n+1,m+1} + 2v_{\xi\eta}^{n+1,m+1}\eta_x + v_{\eta\eta}^{n+1,m+1}\big(\eta_x^2 + \eta_r^2\big) + v_\eta^{n+1,m+1}\eta_{xx} \\
&\qquad + \frac{1}{r}v_\eta^{n+1,m+1}\eta_r - \frac{v^{n+1,m+1}}{r^2}\Big] \\
&\qquad - u^{n+1,m}\big(v_\xi^{n+1,m+1} + v_\eta^{n+1,m+1}\eta_x\big) \\
&\qquad - v^{n+1,m}v_\eta^{n+1,m+1}\eta_r - p_\eta^{n+1,m}\eta_r - \frac{\alpha_w^2}{2\pi R}v_\eta^{n+1,m}\eta_t,
\end{aligned} \tag{4.6}$$

$$\begin{aligned}
&\frac{p^{n+1,m+1} - p^{n+1,m}}{\Delta\sigma} \\
&\quad = -\beta\left(u_\xi^{n+1,m+1} + u_\eta^{n+1,m+1}\eta_x + \frac{v^{n+1,m+1}}{r} + v_\eta^{n+1,m+1}\eta_r\right),
\end{aligned} \tag{4.7}$$

where the last terms in (4.5)–(4.6) were due to the presence of t in (4.1). Equations (4.5)–(4.6) were solved using the ADI method, and (4.7) was used to adjust p.

The ADI method. Omitting the superscripts $n+1$ and m and using "$-$" to mark the variables at the $m+1$ level (to be solved for), the discretized iterative scheme for (4.5)–(4.7) in terms of (ξ,η) is given by

(4.8)
$$\begin{aligned}
&\frac{\alpha_w^2}{2\pi R}\frac{1.5\overline{u}(i,j)}{\Delta t}\\
&\quad=\frac{1}{R}\Bigg[\frac{\overline{u}(i+1,j)+\overline{u}(i-1,j)-2\overline{u}(i,j)}{\Delta\xi^2}\\
&\qquad+2\frac{\overline{u}(i+1,j+1)-\overline{u}(i+1,j-1)-\overline{u}(i-1,j+1)+\overline{u}(i-1,j-1)}{\Delta\xi\Delta\eta}\eta_x\\
&\qquad+\frac{\overline{u}(i,j+1)+\overline{u}(i,j-1)-2\overline{u}(i,j)}{\Delta\eta^2}\big(\eta_x^2+\eta_r^2\big)+\frac{\overline{u}(i,j+1)-\overline{u}(i,j-1)}{2\Delta\eta}\eta_{xx}\\
&\qquad+\frac{\overline{u}(i,j+1)-\overline{u}(i,j-1)}{2r\Delta\eta}\eta_r\Bigg]\\
&\quad-u\big(u_\xi+u_\eta\eta_x\big)-vu_\eta\eta_r-\big(p_\xi+p_\eta\eta_x\big)\\
&\quad+\frac{\alpha_w^2}{2\pi R}\frac{2u^n(i,j)-0.5u^{n-1}(i,j)}{\Delta t}-\frac{\alpha_w^2}{2\pi R}u_\eta\eta_t,
\end{aligned}$$

(4.9)
$$\begin{aligned}
&\frac{\alpha_w^2}{2\pi R}\frac{1.5\overline{v}(i,j)}{\Delta t}\\
&\quad=\frac{1}{R}\Bigg[\frac{\overline{v}(i+1,j)+\overline{v}(i-1,j)-2\overline{v}(i,j)}{\Delta\xi^2}\\
&\qquad+2\frac{\overline{v}(i+1,j+1)-\overline{v}(i+1,j-1)-\overline{v}(i-1,j+1)+\overline{v}(i-1,j-1)}{\Delta\xi\Delta\eta}\eta_x\\
&\qquad+\frac{\overline{v}(i,j+1)+\overline{v}(i,j-1)-2\overline{v}(i,j)}{\Delta\eta^2}(\eta_x^2+\eta_r^2)+\frac{\overline{v}(i,j+1)-\overline{v}(i,j-1)}{2\Delta\eta}\eta_{xx}\\
&\qquad+\frac{\overline{v}(i,j+1)-\overline{v}(i,j-1)}{2r\Delta\eta}\eta_r-\frac{\overline{v}(i,j)}{r^2}\Bigg]\\
&\quad-u\big(v_\xi+v_\eta\eta_x\big)-vv_\eta\eta_r-p_\eta\eta_r\\
&\quad+\frac{\alpha_w^2}{2\pi R}\frac{2v^n(i,j)-0.5v^{n-1}(i,j)}{\Delta t}-\frac{\alpha_w^2}{2\pi R}v_\eta\eta_t,
\end{aligned}$$

$$\overline{p}(i,j)=p(i,j)-\gamma\left(\overline{u}_\xi+\overline{u}_\eta\eta_x+\frac{\overline{v}}{r}+\overline{v}_\eta\eta_r\right), \tag{4.10}$$

where $\Delta\xi$ and $\Delta\eta$ are step sizes in ξ and η directions, all quantities were evaluated at (i,j) (i.e., the point $(\xi_i,\eta_j)=(i\cdot\Delta\xi,j\cdot\Delta\eta)$ unless otherwise specified), and $\gamma=\Delta\tau\cdot\beta$ is an iteration constant.

This difference system is very expensive to solve because each equation involves nine unknowns. We applied the ADI technique to reduce the system to two tridiagonal

systems that can be solved very efficiently [10]. For each i fixed, the function at other i values were treated as known and the following tridiagonal system was solved:

$$A_u(i,j)\overline{u}(i,j-1)+B_u(i,j)\overline{u}(i,j)+C_u(i,j)\overline{u}(i,j+1)=D_u(i,j), \tag{4.11}$$

$$A_v(i,j)\overline{v}(i,j-1)+B_v(i,j)\overline{v}(i,j)+C_v(i,j)\overline{v}(i,j+1)=D_v(i,j), \tag{4.12}$$

where

$$A_u(i,j)=\frac{1}{R}\left[\frac{\eta_{xx}}{2\Delta\eta}+\frac{\eta_r}{2r\Delta\eta}-\frac{\eta_x^2+\eta_r^2}{\Delta\eta^2}\right], \tag{4.13}$$

$$B_u(i,j)=\frac{\alpha_w^2}{2\pi R}\frac{3}{2\Delta t}+\frac{2}{R}\left[\frac{1}{\Delta\xi^2}+\frac{\eta_x^2+\eta_r^2}{\Delta\eta^2}\right], \tag{4.14}$$

$$C_u(i,j)=-\frac{1}{R}\left[\frac{\eta_{xx}}{2\Delta\eta}+\frac{\eta_r}{2r\Delta\eta}+\frac{\eta_x^2+\eta_r^2}{\Delta\eta^2}\right], \tag{4.15}$$

$$\begin{aligned}D_u(i,j)=&\frac{1}{R}\left[\frac{u(i+1,j)+u(i-1,j)}{\Delta\xi^2}+2u_{\xi\eta}\eta_x\right]-u\big(u_\xi+u_\eta\eta_x\big)-vu_\eta\eta_r\\&-\big(p_\xi+p_\eta\eta_x\big)+\frac{\alpha_w^2}{2\pi R}\frac{2u^n(i,j)-0.5u^{n-1}(i,j)}{\Delta t}-\frac{\alpha_w^2}{2\pi R}u_\eta\eta_t,\end{aligned} \tag{4.16}$$

$$A_v=A_u,\qquad B_v=B_u+\frac{1}{Rr^2},\qquad C_v=C_u, \tag{4.17}$$

$$\begin{aligned}D_v(i,j)=&\frac{1}{R}\left[v\frac{(i+1,j)+v(i-1,j)}{\Delta\xi^2}+2v_{\xi\eta}\eta_x\right]-u\big(v_\xi+v_\eta\eta_x\big)\\&-vv_\eta\eta_r-p_\eta\eta_r+\frac{\alpha_w^2}{2\pi R}\frac{2v^n(i,j)-0.5v^{n-1}(i,j)}{\Delta t}-\frac{\alpha_w^2}{2\pi R}v_\eta\eta_t.\end{aligned} \tag{4.18}$$

For each j fixed, the system can be handled similary. Equation (4.10) is used to compute $\overline{p}(i,j)$ each time u and v are updated.

Regularized central difference scheme. It is known that the central difference scheme is nonregular [16], which results in nonsmooth solutions. To overcome this difficulty, the following difference formulas of third-order accuracy were used for the first-order derivatives of space variables to obtain regularized scheme [16, 17]:

$$f_\xi(i,j)=\delta_{\xi o}f-\frac{1}{6}\Delta\xi^2\delta_{\xi-}\delta_{\xi+}^2 f, \tag{4.19}$$

$$f_\eta(i,j)=\delta_{\eta o}f-\frac{1}{6}\Delta\eta^2\delta_{\eta-}\delta_{\eta+}^2 f, \tag{4.20}$$

where

$$\big(\delta_{\xi o}f\big)(i,j)=\frac{[f(i+1,j)-f(i-1,j)]}{(2\Delta\xi)}, \tag{4.21}$$

$$\big(\delta_{\xi+}f\big)(i,j)=\frac{[f(i+1,j)-f(i,j)]}{\Delta\xi}, \tag{4.22}$$

$$\big(\delta_{\xi-}f\big)(i,j)=\frac{[f(i,j)-f(i-1,j)]}{\Delta\xi}, \tag{4.23}$$

and the corresponding differences for η can be defined similary.

Boundary conditions. We impose periodic boundary conditions on u and v and the pressure-drop condition for p in the ξ-direction. At $\eta=0$ and $\eta=1$, cubic

TABLE 1

Relative residuals of equations by the numerical solutions; order of accuracy of the numerical method. $p_0 = 100$, $p_{do} = 50$, $R = 10$, $S_0 = 0.5$, $K_{pi} = 20$, $\lambda_{kp} = 0$, $A_{pe} = 0.5$, $T = 1$, $t = 3T$, $\alpha_w = 3.54$.

m	n	(4.8)	(4.9)	(4.10)	(2.18)
40	6	0.000294	0.000312	0.000541	0.000384
80	12	0.000105	0.000093	0.000113	0.000112
160	24	0.000053	0.000042	0.000075	0.000068

interpolation was used for pressure:

$$p(i,0) = 3\big(p(i,1) - p(i,2)\big) + p(i,3), \tag{4.24}$$

$$p(i,n) = 3\big(p(i,n-1) - p(i,n-2)\big) + p(i,n-3). \tag{4.25}$$

Boundary condition (2.17) was used for (u, v) at $\eta = 1$. At $\eta = 0$, we set

$$\frac{\partial u}{\partial r} = 0, \qquad v = 0. \tag{4.26}$$

Computing grids, procedure, and stopping criterions. In the computation, $\Delta\xi$ and $\Delta\eta$ were set at 0.0625 and 0.05, respectively, for a mesh of 160×20. The algorithm contains three processes: the local iteration to solve the Navier–Stokes equations over a given domain indicated by index m, the boundary iteration indicated by index k (omitted in the equations for simplicity) to deal with the unknown boundary, and the real-time advancing indicated by n. The boundary iterations were stopped when the relative residuals of the equations (4.8)–(4.10) and the tube law (2.18) became less than 10^{-4}. About 20 boundary iterations were needed for the beginning time steps to reach the desired accuracy. After one time period, only 2 to 5 boundary iterations were needed for each time step to achieve the same accuracy. The solutions were considered periodic when the pointwise difference of velocity, pressure, and boundary between the last two periods became less than 10^{-3}. Then the last periods of the solutions were considered the periodic solutions of the exact system.

5. Results and discussions. Extensive computations were conducted to study the fluid mechanics of this interesting phenomenon. Parameters such as the severity of the stenosis S_0, mean pressure drop p_{do}, the relative pulsatile pressure wave amplitude A_{pe}, and the Reynolds number R were varied to study the wall motion, pressure, and flow behaviors. Special attention was given to the boundary changes because tube wall contraction is an indication of possible wall collapsing and tube expansion distal to stenosis is an indication of possible tube reopening after collapse.

In this numerical example, we set $R_0 = 0.5$, $\ell = 10$, $x_1 = 3.45$, $x_2 = 6.55$, $n_1 = 5$, $n_2 = 1.5$, $k_{pi} = 20$, $R = 0.1 - 100$, $\alpha_w = 3.54$, $T = 1$. For the periodic solutions, four observation times $t_k = (\frac{k-1}{4})T, k = 1, \ldots, 4$, were chosen to present the time-dependent behavior of the solutions.

5.1. Accuracy of the method and comparison between the longwave solutions and the numerical solutions. Equations (4.8)–(4.10) were solved over the (ξ, η)-domain $[0, 10] \times [0, 1]$ using three different grids ($m \times n = 40 \times 6, 80 \times 12$, and 160×24, respectively) to check the accuracy of the numerical method. The relative residuals of the equations (4.8)–(4.10) and the tube law (2.18) are given in Table 1.

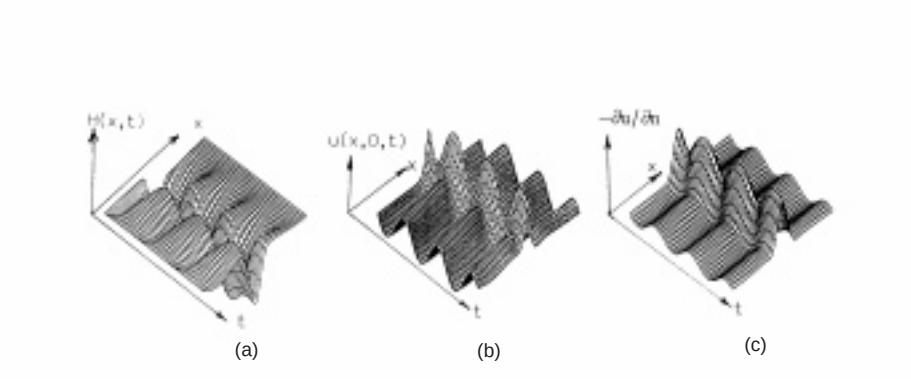

FIG. 2. *Graphs of tube radius H, axial velocity u at centerline, and shear rate $-\partial u/\partial n$ at the tube wall as functions of x and t. $S_0 = 0.6$, $p_0 = 100$, $p = 100$, $A_{pe} = 0.5$, $R = 10$, $\alpha_w = 3.54$.*

Relative residuals are defined as

$$\frac{\|\text{residual of equation}(\cdot)\|_2}{\|f\|_2},$$

where f is u, v, p, and H for equations (4.8)–(4.10) and the tube law (2.18), respectively.

To compare the longwave approximations with the numerical solutions, we set $A_{pe} = 0$, so that the model became steady and computations were conducted until steady solutions were obtained and the relative residuals became less than 10^{-4}. The L_2 norms of the relative differences between the longwave approximations and the numerical solutions are given by Table 2 for severities $S_0 = 0.1 - -0.9$. The results indicate that the longwave solutions gave reasonable approximations when S_0 was small. Table 2 also shows that the longwave approximations became practically invalid for severe stenotic cases.

TABLE 2

Comparisons of longwave approximations with numerical solutions. $p_0 = 100$, $p_{do} = 60$, $R = 1.0$, $k_{pi} = 20$, $\lambda_{kp} = 0.0$, $A_{pe} = 0.0$, $m = 160$, $n = 20$. u_0, v_0, p^0, and H^0 are longwave approximations.

S_0	$\|u-u_0\|_2/\|u\|_2$	$\|v-v_0\|_2/\|v\|_2$	$\|p-p^0\|_2/\|p\|_2$	$\|H-H^0\|_2/\|H\|_2$
0.1	0.026386	0.055881	0.015619	0.005268
0.2	0.067283	0.103892	0.039838	0.011563
0.3	0.114790	0.134321	0.082232	0.018296
0.4	0.172124	0.166645	0.151775	0.025004
0.5	0.238611	0.205646	0.225218	0.029192
0.6	0.293133	0.293657	0.264862	0.029723
0.7	0.356346	0.398325	0.276110	0.026312
0.8	0.414449	0.478405	0.285784	0.023434
0.9	0.458283	0.527972	0.519607	0.021933

5.2. A brief overview of the solution. Three periods of the wall motion, axial velocity at the centerline of the tube, and the shear rate $-\partial u/\partial n$ at the tube wall were plotted for a typical case with $S_0 = 0.6$, $p_0 = 100$, $p_{do} = 100$, $A_{pe} = 0.5$, $R = 10$, and $\alpha_w = 3.54$. Figure 2(a) shows the boundary moves corresponding to the

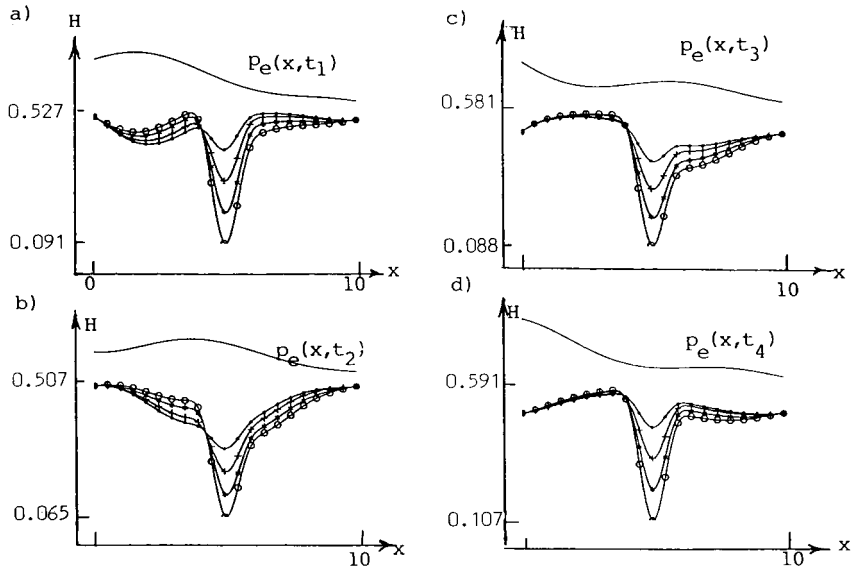

FIG. 3. *Tube radius $H(x,t_k)$ with four stenosis severity S_0 values at $t = t_k = kT/4$, $k = 1,2,3,4$. Markers: $\bullet\bullet\bullet$: $S_0 = 0.2$; $+++$: $S_0 = 0.4$, $***$: $S_0 = 0.6$; $\circ\circ\circ$: $S_0 = 0.8$. $p_0 = 100$, $p_{do} = 100$, $A_{pe} = 0.5$, $R = 10$, $K_{pi} = 20$, $\lambda_{kp} = 0.0$, $T = 1$, $\alpha_w = 3.54$.*

imposed pressure conditions. Figure 2(b) shows that the axial velocity reached its maximum at the throat. Shear rate obtained its maximum at the stenosis, as shown by Figure 2(c). Detailed information can be obtained from the velocity field and shear rate field, respectively.

5.3. Effect of severity of stenoses on the tube wall. It has been shown that the stenotic tube expands at the proximal side of the stenosis and contracts just distal to the stenosis under steady flow conditions [19]. The expansion and contraction become very noticeable when stenosis severity S_0 exceeds a critical value, which was found to be around 0.6. These are called static expansions and contractions.

In order to see the wall behavior under the unsteady pressure condition, computations were carried out for flow in tubes with $S_0 = 0.2, 0.4, 0.6, 0.8$. Figure 3 compares the $H(x)$ curves with different S_0 values at the observation times specified before. Tube expansions and contractions were observed before and after the stenoses and were complicated by the imposed pulsatile pressure conditions. The external pressure was plotted in each graph to provide easy reference.

At $t = t_1$, the peak of the imposed external pressure was within the first quarter of the tube length. As a consequence, the tube wall was compressed and tube contraction was observed proximal to the stenosis. Tubes with more severe stenoses showed less contraction because part of the contraction force was canceled by the static expansion force due to severe stenosis. Distal to the stenosis, tubes with $S_0 < 0.6$ showed expansion, whereas tubes with $S_0 = 0.8$ showed contraction.

It is worth noting that the order of the curves was switched before and after the stenosis. The curves with more severe stenosis were above the curves with less severe stenosis proximal to the stenosis. Then there is a switch point in the graph after which

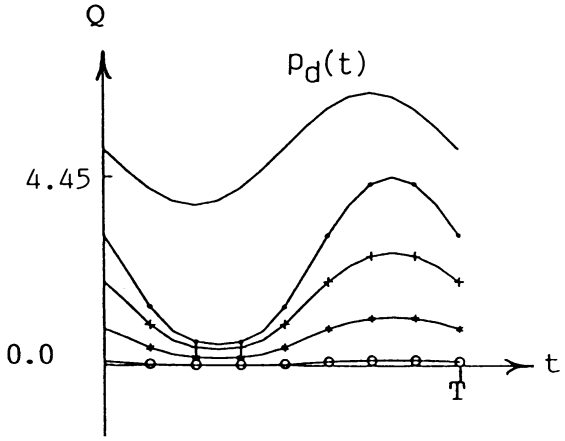

FIG. 4. *Tube flux $Q(\ell/2, t)$ at the stenoses with $S_0 = 0.2, 0.4, 0.6, 0.8$. Markers: $\bullet\bullet\bullet$: $S_0 = 0.2$; $+++$: $S_0 = 0.4$; $***$ $S_0 = 0.6$; $\circ\circ\circ$: $S_0 = 0.8$. $p_0 = 100$, $p_{do} = 100$, $A_{pe} = 0.5$, $R = 10$, $K_{pi} = 20$, $\lambda_{kp} = 0.0$, $T = 1$, $\alpha_w = 3.54$.*

the curves with more severe stenosis were below the curves with less severe stenosis. This is because the tube with more static expansion proximal to the stenosis also has more static contraction distal to the stenosis.

At $t = t_2$, the peak of the imposed external pressure was within the second quarter of the tube length. The contraction force from the pressure overcame the static expansion just proximal to the stenosis. As a consequence, the tube wall was contracted almost for the entire length.

At $t = t_3$, the peak of the imposed external pressure moved to the third quarter of the tube length. The contraction force from the pressure enhanced the static tube contraction distal to the stenosis. It should also be noticed that the valley of the pressure wave was at the static expansion region and therefore also enhanced the tube expansion there. As a consequence, the wall expansion and contraction were both enhanced for the entire length of the tube.

At $t = t_4$, the valley (minimum) of the pressure wave was at the second quarter of the tube length. Therefore, the tube wall expansion was enhanced there. Static tube contraction distal to the stenosis was weakened for the same reason.

The complicated wall motion can be understood as the superposition of the static expansion and contraction caused by stenosis and the unsteady motion caused by the imposed external pressure wave. Wall contraction became more severe when both the static and unsteady contractions were enhancing each other. The presence of wall expansion distal to the stenosis caused by the imposed pressure wave can be the possible mechanism for tube reopening after collapsing.

Figure 4 shows that the flux Q varied the same way as the imposed pressure drop given by (2.27). It is clear that severity of stenosis also has a considerable effect on the flow rate.

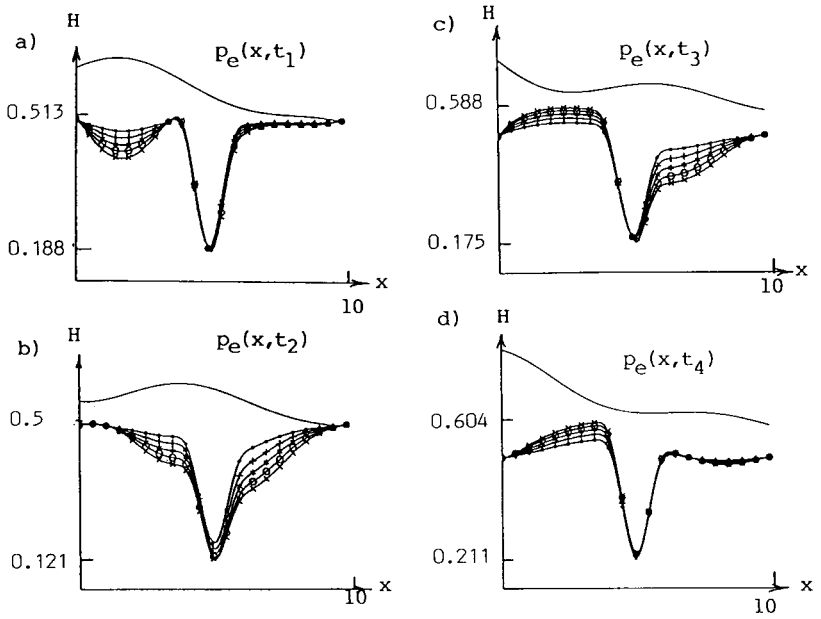

FIG. 5. *Tube radius curves* $H(x,t_k)$ *with* $p_{do} = 50, 75, 100, 125,$ *and* 150 *at* $t = t_k$, $k = 1, 2, 3, 4$. *Markers:* $\bullet\bullet\bullet$*:* $p_{do} = 50$*;* $+++$*:* $p_{do} = 75$*;* $***$*:* $p_{do} = 100$*;* $\circ\circ\circ$*:* $p_{do} = 125$*;* $\times\times\times$*:* $p_{do} = 150$. $S_0 = 0.6$, $p_0 = 100$, $A_{pe} = 0.5$, $R = 10$, $K_{pi} = 20$, $\lambda_{kp} = 0.0$, $T = 1$, *and* $\alpha_w = 3.54$.

5.4. Effects of p_{do} and A_{pe} on the wall motion. The flow was driven by the pressure drop $p_d(t)$ and external pressure $p_e(x,t)$, which are related by (2.24)–(2.27). Two parameters p_{do} and A_{pe} were used to prescribe the pressure conditions. To see the effects of p_{do}, computations were performed for $p_{do} = 50, 75, 100, 125$, and 150 for flow in a stenotic tube with $S_0 = 0.6$ and $A_{pe} = 0.5$. Figure 5 shows that a larger p_{do} caused greater wall expansions and contractions. $p_{do} = 150$ caused about 20% tube contraction while the contraction caused by $p_{do} = 50$ was only about 7.5%. For the four time values, the wall motion behavior was similar to what is shown in Figure 2 and the discussion is omitted here.

Computations were conducted for $A_{pe} = 0.0, 0.25, 0.5$, and 0.75 to see the effect of A_{pe} on wall motion and flow behaviors. To see the wall motions more clearly, the boundary variation curves $H_c(x,t_k)$ of different A_{pe} values were plotted in Figure 6. As t changed from t_1 to t_4 and the pressure wave traveled along the tube, corresponding tube wall expansions and contractions similar to Figures 2 and 5 were observed. It is clear that larger A_{pe} values corresponded to considerably larger wall expansions (13% for $A_{pe} = 0.75$ vs. 5% for $A_{pe} = 0$) and contractions (21.6% for $A_{pe} = 0.75$ vs. only 6% for $A_{pe} = 0$). This indicated that tube wall collapse has a much higher chance for larger A_{pe} values.

5.5. Effect of the Reynolds number on the flow. Computations were done for $R = 1$, 10, and 100 to observe the effect of the Reynolds number on the flow. Figure 7(a) contains the three boundary curves for $R = 1, 10$, and 100. They coincide with each other. The centerline velocity $u(x,0,t)$ at $t = t_1$, flux $Q(t)$, and shear rate $-\partial u/\partial n$ at the tube wall with $x = \ell/2$ were given by Figures 7(b) to 7(d). Other

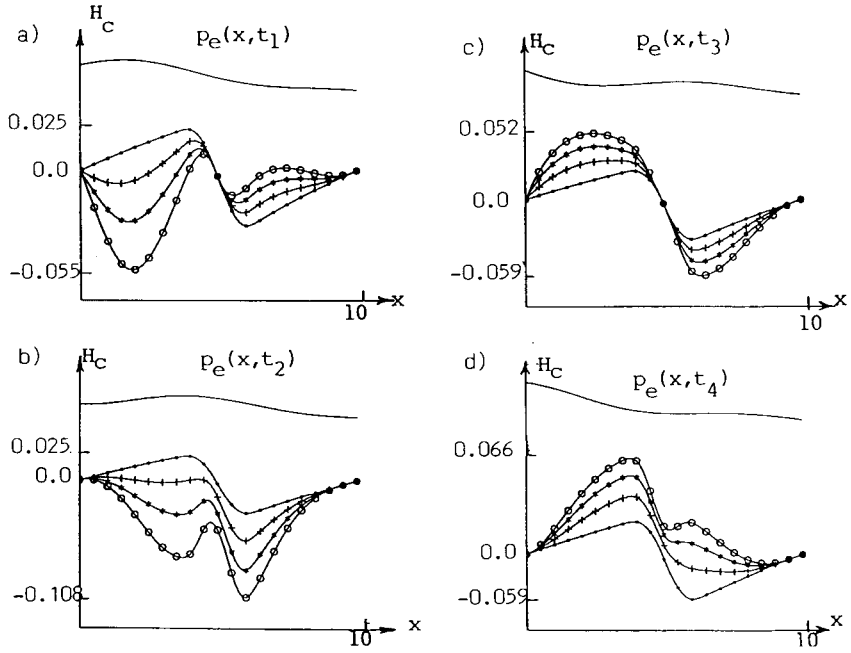

FIG. 6. *Changes of tube radius* $H_c(x,t_k)$ *with* $A_{pe}=0,0.25,0.5,0.75$ *at* $t=t_k$, $k=1,2,3,4$. *Markers:* $\bullet\bullet\bullet$*:* $A_{pe}=0$*;* $+++$*:* $A_{pe}=0.25$*;* $***$*:* $A_{pe}=0.5$*;* $\circ\circ\circ$*:* $A_{pe}=0.75$. $S_0=0.6$, $p_0=100$, $p_{do}=50$, $R=10$, $K_{pi}=20$, $\lambda_{kp}=0.0$, $T=1$, *and* $\alpha_w=3.54$.

than the boundaries, all the curves show that the Reynolds number had considerable influences on the flow quantitatively. However, the behaviors of those curves in each group with different R values were all qualitatively similar to each other.

5.6. Effect of stiffness variation of stenoses on the flow. The presence of stenosis may effect the stiffness of the tube wall, which in turn will have influence over the flow. To check on this, computation was conducted with $\lambda_{kp}=0.5,0.0$, and -0.5. When $\lambda_{kp}=0.5$, the stenosis made the tube stiffer while stenosis with $\lambda_{kp}=-0.5$ made the tube softer. It was found that the effect of λ_{kp} in this model was very limited. The corresponding graphs basically show no differences for the three cases and are therefore omitted in this paper [19].

5.7. Comparison between the steady and unsteady solutions: Transmural pressure and wall contractions and expansions. Figure 8 shows the steady and unsteady transmural pressure P_{tran} and the tube radius variation H_c for $t=t_1$ and t_3 and stenosis severities $S_0=0.4,0.6$, and 0.8. The darker lines are for the steady solutions. The unsteady solutions were plotted for $t=t_1$ and t_3, each giving maximum contraction and expansion, respectively. Maximum tube expansions and contractions are given in Table 3. While the steady solutions showed that more severe stenosis caused more tube expansions and contractions, the unsteady effect is much more noticeable. While the steady tube contraction and expansion for $S_0=0.8$ were 8.64% and 5.72%, respectively, the unsteady tube contractions and expansions were 23.4% and 13.5%, almost three times as much as the steady case. The unsteady pressure conditions certainly play a vital role in the tube collapsing process.

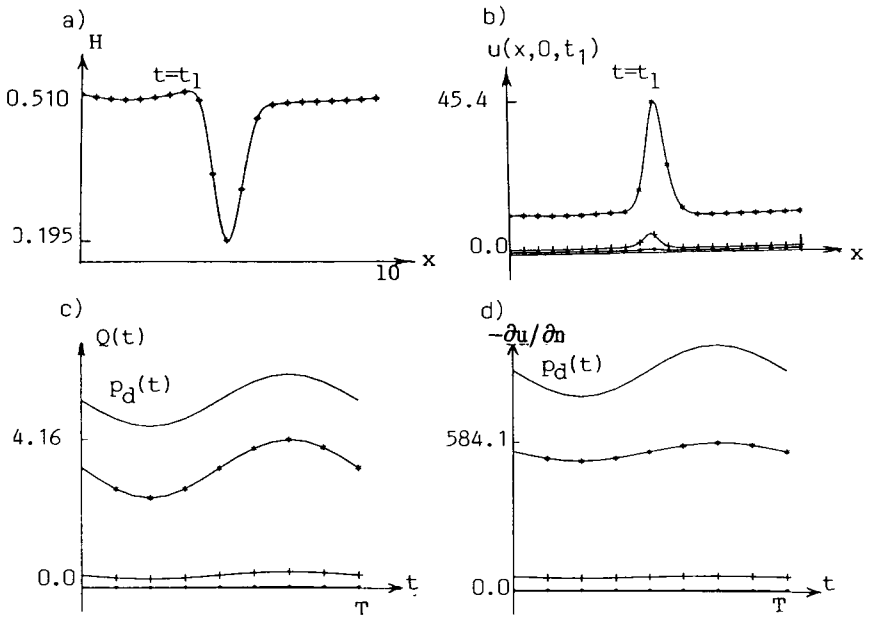

FIG. 7. *Effects of Reynolds number changes on the tube wall, velocity, flux, and shear rate.* $S_0 = 0.6$, $p_0 = 100$, $p_{do} = 50$, $A_{pe} = 0.3$, $K_{pi} = 20$, $\lambda_{kp} = 0.0$, $T = 1$, *and* $\alpha_w = 3.54$. *Markers:* $\bullet\bullet\bullet$*:* $R = 1$; $+++$*:* $R = 10$; $***$*:* $R = 100$.

TABLE 3

Comparisons between steady and unsteady solutions. $p_0 = 100, p_{do} = 50, R = 10, k_{pi} = 20, \lambda_{kp} = 0.0, T = 1, \alpha_w = 3.54, A_{pe} = 0.0$ *(steady cases) and* 0.75 *(unsteady cases).*

		Tube radius variation H_c				Transmural pressure	
S_0	st/unst cases	max (expansion)		min (contraction)		max	min
0.4	Steady	0.118	(2.26%)	-0.0140	(2.8%)	6.96	-7.18
	Unsteady	0.0586	(11.7%)	-0.0904	(18.1%)	47.81	-40.75
0.6	Steady	0.0217	(4.34%)	-0.0296	(5.92%)	14.23	-14.66
	Unsteady	0.638	(12.8%)	-0.1058	(21.2%)	55.04	-48.42
0.8	Steady	0.0286	(5.72%)	-0.0432	(8.64%)	21.06	-21.63
	Unsteady	0.0676	(13.5%)	-0.1170	(23.4%)	61.32	-56.63

6. Conclusions. We conclude the following from the above observations. (a) Severity of stenoses has a much more noticeable effect on the flow and wall motion under unsteady conditions. (b) Pulsatile pressure conditions cause unsteady tube contractions and expansions. The peak wall contractions and expansions are much more severe than the static ones (see Table 3). Therefore, tube collapsing and reopening are more likely to occur under pulsatile pressure conditions. (c) Greater pressure drop causes more severe tube contraction and expansion. (d) Change of Reynolds number has a considerable effect on the flow properties. Solutions with different R-values behave similarly, with quantities changing with R proportionally.

These findings provide evidence that stenosis severity and unsteady pressure conditions are important factors affecting the tube collapsing and reopening in stenotic collapsible tubes. Further research using three-dimensional models is needed so that

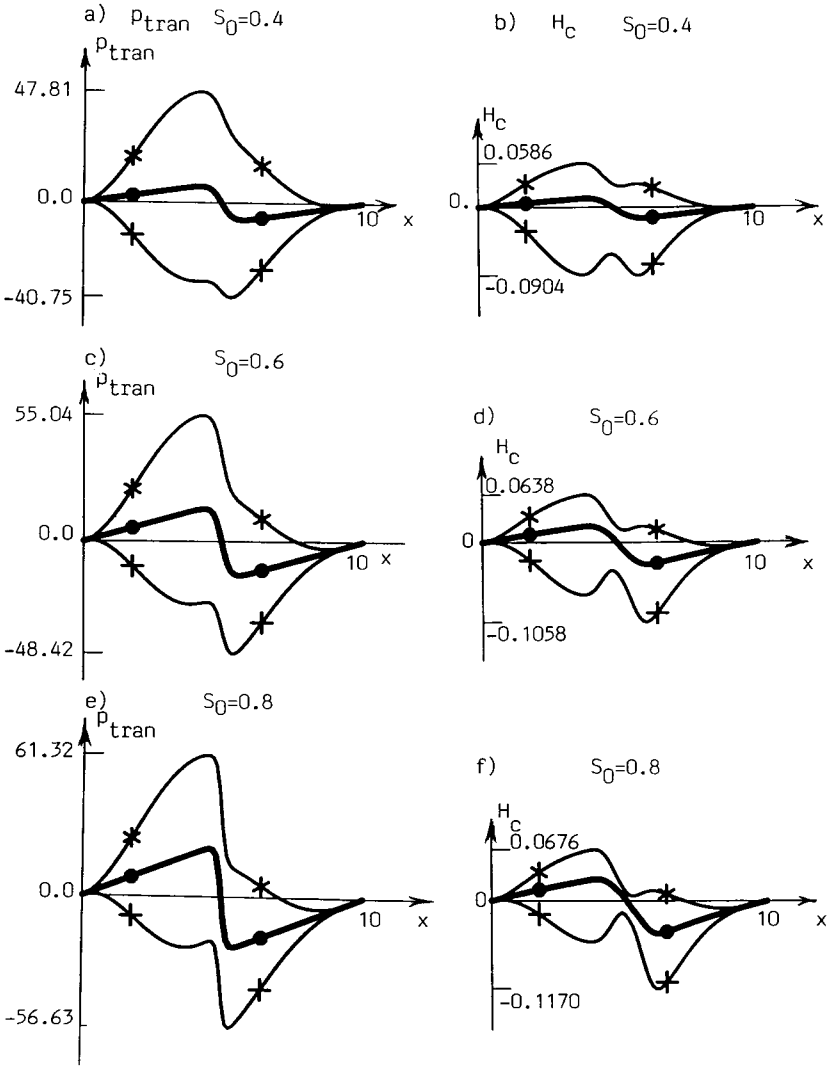

FIG. 8. *Comparisons between the steady and unsteady solutions. Plots of transmural pressure across the tube wall* $(p - p_e)$ *and tube radius variations* $H_c(x, t_k)$ *at* $t = t_1$ *and* t_3*; Markers:* $\bullet\bullet\bullet$*: steady solution;* $+++$*:* $t = t_1$*;* $***$*:* $t = t_3$*.* $p_0 = 100$*,* $p_{do} = 50$*,* $R = 10$*,* $K_{pi} = 20$*,* $\lambda_{kp} = 0.0$*,* $T = 1$*, and* $\alpha_w = 3.54$*, and* $A_{pe} = 0.75$ *for the unsteady case.*

the results can be more realistic and physiologically relevant, and so that tube collapsing can be observed.

REFERENCES

[1] T. AOKI AND D. N. KU, *Collapse of diseases arteries with eccentric cross section*, J. Biomech., 26 (1993), pp. 133–142.

[2] R. L. BINNS AND D. N. KU, *Effect of stenosis on wall motion*, Arteriosclerosis, 9 (1989), pp. 842–847.

[3] J. M. DOWNING, *Flow Through a Compliant Stenotic Artery: A Parametric Evaluation*, Ph.D.

thesis, Georgia Institute of Technology, Atlanta, 1993.
[4] L. J. Fauci, *Peristaltic pumping of solid particles*, Comput. Fluids, 21 (1992), pp. 583–598.
[5] Y. C. Fung, *Biodynamics: Circulation*, Springer-Verlag, New York, 1984.
[6] R. D. Kamm and A. H. Shapiro, *Unsteady flow in a collapsible tube subjected to external pressure or body force*, J. Fluid Mech., 95 (1979), pp. 1–78.
[7] D. N. Ku, D. P. Giddens, D. J. Phillips, and D. E. Strandness, Jr., *Hemodynamics of the normal human carotid bifurcation: In vitro and in vivo studies*, Ultrasound in Med. Biol., 11 (1985), pp. 13–26.
[8] D. N. Ku, D. P. Giddens, C. K. Zarins, and S. Glagov, *Pulsatile flow and atherosclerosis in the human carotid bifurcation: Positive correlation between plaque location and low and oscillating stress*, Arteriosclerosis, 5 (1985), pp. 293–302.
[9] D. N. Ku, M. N. Zeigler, and J. M. Downing, *One-dimensional steady inviscid flow through a stenotic collapsible tube*, J. Biomech. Engrg., 112 (1990), pp. 444–450.
[10] D. Kwak, *Computation of Viscous Incompressible Flows*, NASA Technical Memorandum 101090, Ames Research Center, Moffett Field, CA, 1989.
[11] B. Liu and D. Tang, *A finite element solution of viscous flow in stenotic elastic tubes under an external pressure and longitudinal tension*, Biomech. Engrg., (1996), pp. 191–192.
[12] C. S. Peskin, *Numerical analysis of blood flow in the heart*, J. Comput. Phys., 25 (1977), pp. 220–252.
[13] C. S. Peskin, *A three-dimensional computational method for blood flow in the heart*, J. Comput. Phys., 81 (1989), pp. 372–405.
[14] M. E. Rosar, *A Three-Dimensional Computer Model for Fluid Flow Through a Collapsible Tube*, Ph.D. thesis, New York University, 1995.
[15] A. H. Shapiro, *Steady flow in collapsible tubes*, ASME J. Biomech. Engrg., 99 (1977), pp. 126–147.
[16] J. C. Strikwerda, *Finite difference methods for the Stokes and Navier–Stokes equations*, SIAM J. Sci. Stat. Comput., 5 (1984), pp. 56–68.
[17] J. C. Strikwerda, *Finite Difference Schemes and Partial Differential Equations*, Chapman and Hall, New York, 1989.
[18] D. Tang and S. Rankin, *Numerical and asymptotic solutions for peristaltic motion of nonlinear viscous flows with elastic free boundaries*, SIAM J. Sci. Comput., 14 (1993), pp. 1300–1319.
[19] D. Tang, *Numerical solutions of viscous flow in elastic tubes with stenoses of various stiffness*, Proceedings of 1995 Bioengineering Conference, ASME, Bioengineering Division, Vol. 29, 1995, pp. 521–522.
[20] J.-M. Vanden-Broek, *Nonlinear gravity-capillary standing waves in water of arbitrary uniform depth*, J. Fluid. Mech., 139 (1984), pp. 97–104.
[21] J.-M. Vanden-Broeck and J. B. Keller, *Free surface flow due to a sink*, J. Fluid Mech., 175 (1987), pp. 109–117.